# **Inorganic Chemistry**

pubs.acs.org/IC Article

# It Runs in the $BaAl_4$ Family: Relating the Structure and Properties of Middle Child $Ln_2Co_3Ge_5$ (Ln = Pr, Nd, and Sm) to its Siblings $LnCo_2Ge_2$ and $LnCoGe_3$

Trent M. Kyrk, Jan P. Scheifers, Kulatheepan Thanabalasingam, Gregory T. McCandless, David P. Young, and Julia Y. Chan\*



Cite This: Inorg. Chem. 2021, 60, 15343-15350



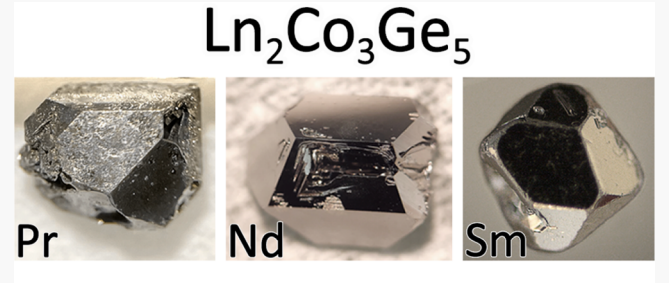
ACCESS

Metrics & More

Article Recommendations

Supporting Information

**ABSTRACT:** The BaAl<sub>4</sub> prototype structure and its derivatives have been identified to host several topological quantum materials and noncentrosymmetric superconductors. Single crystals up to  $\sim$ 3 mm  $\times$  3 mm  $\times$  5 mm of Ln<sub>2</sub>Co<sub>3</sub>Ge<sub>5</sub> (Ln = Pr, Nd, and Sm) are obtained via flux growth utilizing Sn as metallic flux. The crystal structure is isostructural to the Lu<sub>2</sub>Co<sub>3</sub>Si<sub>5</sub> structure type in the crystallographic space group C2/c. The temperature-dependent magnetization indicates magnetic ordering at 30 K for all three compounds. Pr<sub>2</sub>Co<sub>3</sub>Ge<sub>5</sub> and Nd<sub>2</sub>Co<sub>3</sub>Ge<sub>5</sub> exhibit complex magnetic behavior with spin reorientations before ordering antiferromagnetically around 6 K, whereas Sm<sub>2</sub>Co<sub>3</sub>Ge<sub>5</sub> shows a clear antiferromagnetic behavior at 26 K. The structures and properties



flux growth - structure - physical properties

of  $Ln_2Co_3Ge_5$  (Ln = Pr, Nd, and Sm) are compared to those of the  $ThCr_2Si_2$  and  $BaNiSn_3$  structure types. Herein, we present the optimized crystal growth, structure, and physical properties of  $Ln_2Co_3Ge_5$  (Ln = Pr, Nd, and Sm).

#### 1. INTRODUCTION

Recently, BaAl<sub>4</sub> was identified as topologically nontrivial, sparking interest in isostructural compounds and derivative structures such as ThCr<sub>2</sub>Si<sub>2</sub> and noncentrosymmetric BaNiSn<sub>3</sub> structure types. Electronic structure calculations also identified CeCoGe3, a system to study the interplay of superconductivity and antiferromagnetism, as topologically nontrivial.<sup>2,3</sup> Additionally, calculations have made connections between the superconducting and topological states through Coulombic interactions between the Ce-4f orbitals.<sup>4</sup> The recently discovered structurally complex homologous series  $A_{n+1}B_nX_{3n+1}(A = lanthanide; B = transition metal; X = tetrel)$  is a new family of intergrowth structures<sup>5</sup> with several of the members containing BaNiSn<sub>3</sub> subunits. While we were optimizing the reaction conditions to grow and maximize the yield of members of the homologous series, we grew large single crystals (as shown in Figure 1) of  $Ln_2Co_3Ge_5$  (Ln = Pr, Nd, and Sm) in high yield.

 ${\rm Ln_2M_3Ge_5}$  (Ln = lanthanide element; M = transition metal) is rich in intriguing physical phenomena, with  ${\rm La_2Pt_3Ge_5}$  showing superconductivity and  ${\rm Pr_2Pt_3Ge_5}$  showing superconductivity and antiferromagnetism.<sup>6–8</sup> Another highlight is  ${\rm Sm_2Ru_3Ge_5}$ , which adopts two different polymorphs: one in the  ${\rm Sc_2Fe_3Si_5}$  structure type (P4/mnc) and the other in the  ${\rm U_2Co_3Si_5}$  structure type (Ibam). Each polymorph shows charge density wave order: one at 175 °C and the other at 240 °C, respectively.<sup>9,10</sup> There are six different structure types reported

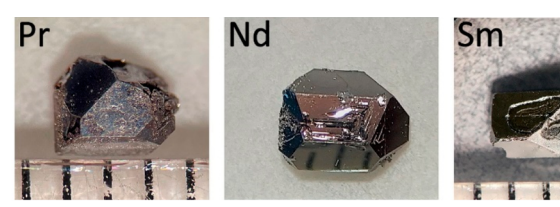


Figure 1. Crystals of  $Ln_2Co_3Ge_5$  as obtained from flux growth in Sn. One mark is equivalent to 1 mm.

for intermetallic tetrels with the formula  $Ln_2M_3X_5$ :<sup>11</sup> two of which are the orthorhombic  $U_2Co_3Si_5^{12}$  and the monoclinic  $Lu_2Co_3Si_5$ -type structures,<sup>13</sup> both distorted supercells of the BaAl<sub>4</sub> prototype.<sup>14</sup>  $Ce_2Co_3Ge_5$  has been identified in the  $U_2Co_3Si_5$  structure type, and its transport and magnetic properties are well reported in powder samples, with Ce understood to be valence instable.<sup>15,16</sup> The  $Pr^{15,17}$  and  $Nd^{18}$  analogues, however, have been previously identified in both the orthorhombic  $U_2Co_3Si_5$  and monoclinic  $Lu_2Co_3Si_5$  (C2/c)

Received: June 30, 2021 Published: October 5, 2021





structure types. <sup>15,19</sup> The Sm analogue adopts the monoclinic structure. <sup>20</sup> Furthermore, only the properties of the  $Pr_2Co_3Ge_5$  orthorhombic analogue have been reported, where it was determined to be paramagnetic. <sup>15</sup> The close structural relationship to other BaAl<sub>4</sub> derivatives and the polymorphism in  $Pr_2Co_3Ge_5$  and  $Nd_2Co_3Ge_5$  motivated us to further investigate the physical properties and crystal chemistry of  $Ln_2Co_3Ge_5$  (Ln = Pr, Nd, and Sm). Herein, we present the crystal growth, magnetic susceptibility, and resistivity of  $Ln_2Co_3Ge_5$  in relation to  $LnCo_2Ge_2$  and  $LnCoGe_3$ .

### 2. EXPERIMENTAL SECTION

**2.1. Synthesis.**  $Ln_2Co_3Ge_5$  (Ln = Pr, Nd, Sm) was prepared using the flux growth method with tin as a metallic nonreactive flux. The elements were combined in a ratio of 3 Ln: 2 Co: 7 Ge: 52 Sn for Ln = Nd and Sm and 3 Ln: 2 Co: 7 Ge: 50 Sn for Ln = Pr, with the total mass of each batch as ~1.5 g for Pr and Nd analogues and ~3 g for the Sm analogue. The elements were each transferred to an alumina Canfield crucible  $^{21}$  and then sealed in fused silica tubes under  $\sim 1/3$ atm of Ar gas. The ampules were placed in a furnace at 300 °C and heated to 1175 °C at a rate of 100 °C/h. The samples were heated at 1175 °C for 24 h and cooled to 815 °C at a rate of 3 °C/h. The reaction ampules were removed, inverted, and centrifuged at 815 °C to remove the excess flux. The residual flux on the crystal surfaces were removed by etching the crystals in diluted HCl. The yield ranges from 50-80%. Additionally, two samples of Pr<sub>2</sub>Co<sub>3</sub>Ge<sub>5</sub> were synthesized by arc-melting the Pr, Co, and Ge pieces in the stoichiometric ratio with a total mass of approximately 0.3 g. Each button was flipped and arc-melted multiple times before being placed in an alumina crucible and sealed in fused silica tubes under  $\sim 1/3$  atm of Ar gas. The weight loss during arc-melting was negligible. From there, samples were annealed at 797 and 1000 °C for 500 h, respectively, in attempts to obtain the U2Co3Si5 structure type. Elemental analysis was also performed and details can be found in the Supporting Information.

**2.2. Structure Determination.** Powder X-ray diffraction was performed using a Bruker D8 Advance diffractometer with Cu  $K\alpha$  radiation ( $\lambda=1.54184$  Å). The powder diffraction data confirm the results of the single crystal refinement for all reported compounds as provided in Figure SI1, SI2, and SI3. Single crystal X-ray diffraction data were obtained at room temperature using a Bruker D8 Quest Kappa single crystal X-ray diffractometer, equipped with an  $I\mu$ S microfocus source (Mo  $K\alpha$ ,  $\lambda=0.71073$  Å), a HELIOS optics monochromator, and a PHOTON II CPAD detector. The Bruker SAINT program was used to integrate the diffraction data, and the intensities were corrected for absorption via a multiscan method implemented in SADABS 2016/2. The structures were solved with the intrinsic phasing methods in SHELXT<sup>23</sup> and subsequently anisotropically refined (full-matrix least-squares on  $F^2$ ) using SHELXL2018.

The crystal structure of Ln<sub>2</sub>Co<sub>3</sub>Ge<sub>5</sub> adopts the monoclinic Lu<sub>2</sub>Co<sub>3</sub>Si<sub>5</sub> structure type and not the related U<sub>2</sub>Co<sub>3</sub>Ge<sub>5</sub> orthorhombic structure type with the space group Ibam. Additional pseudosymmetries were found for the Pr and Nd analogues; however, the symmetry elements do not warrant a change in space group choice. During the visual inspection of the precession images of the Sm and Nd analogues, nonmerohedral twinning along the b-directions was observed. The data were integrated and processed with CELL\_-NOW<sup>25</sup> to identify the twinned domains. It was determined that the second domain of the Sm<sub>2</sub>Co<sub>3</sub>Ge<sub>5</sub> crystal, corresponding to 18.6%, is rotated with respect to the first domain by 179.9° around the reciprocal axis (-0.002 1.000 1.000) and the real axis (0.963 1.000 0.999). For Nd<sub>2</sub>Co<sub>3</sub>Ge<sub>5</sub>, the second domain of 43.87% is rotated by  $179.8^{\circ}$  around the reciprocal axis ( $-0.978 - 0.001 \ 1.000$ ) and real axis (0.002 0.000 1.000) compared to the first domain. The determined unit cell was revised using the data generated from CELL NOW. The data were then reduced with the SAINT software. A multiscan absorption correction was applied with TWINABS<sup>26</sup> implemented in

the Bruker APEX3 software package. An initial structure model was developed with the intrinsic phase model, and the structure refinement was performed with the least-squares refinement method using SHELXL2018 for both twinned domains. The lattice parameters and single crystal refinement statistics can be found in Table 1, while the fractional atomic coordinates and anisotropic displacement parameters are provided in Table SI1.

Table 1. Crystallographic Data and Refinement Parameters of Ln,Co<sub>3</sub>Ge<sub>5</sub> (Ln = Pr, Nd, and Sm)<sup>a</sup>

Empirical formula	Pr <sub>2</sub> Co <sub>3</sub> Ge <sub>5</sub>	$Nd_2Co_3Ge_5$	Sm <sub>2</sub> Co <sub>3</sub> Ge <sub>5</sub>
Space group, crystal system	C2/c	(no. 15), monoc	linic
Lattice parameters			
a (Å)	11.380(3)	11.303(2)	11.2016(19)
b (Å)	11.9341(13)	11.9244(15)	11.8864(14)
c (Å)	5.8500(16)	5.8240(8)	5.7797(15)
$\beta$ (deg)	120.462(9)	120.078(11)	119.759(10)
Volume [ų]	684.8(3)	679.26(19)	668.1(2)
Z		4	
Density [g/cm <sup>3</sup> ]	7.97	8.10	8.37
Absorption coefficient [mm <sup>-1</sup> ]	42.5	43.8	46.5
F(000)	1436	1444	1460
Crystal size [mm³]	0.02 × 0.05 × 0.06	$0.01 \times 0.02 \times 0.03$	0.08 × 0.09 × 0.11
$\theta$ range $[^{\circ}]$	2.7-30.5	2.7-33.3	2.7-30.5
Index range			
h	$-16 \rightarrow 16$	$-17 \rightarrow 15$	<b>-16</b> → <b>13</b>
k	$-17 \rightarrow 16$	$0 \rightarrow 18$	$0 \rightarrow 16$
1	$-8 \rightarrow 8$	$0 \rightarrow 8$	$0 \rightarrow 8$
Number of reflections	11659	1305	1025
Unique reflections	1048	1305	1025
parameters/restraints	49/0	50/0	50/0
R <sub>int</sub>	0.041	0.082	0.060
$\Delta ho_{ m max/min}$	1.39/-1.11	2.88/-3.61	1.79/-2.27
GoF	1.16	1.08	1.15
$R\left[F^2>2\sigma(F^2)\right]$	0.015	0.035	0.024
$wR_2(F^2)$	0.036	0.080	0.058
${}^{a}R = \sum_{c}  ( F_{o}  -  F_{c} ) /[(F_{o})^{2}]^{2}\}^{1/2}.$	$\sum  F_o $ and wR	$_{2}=\{\sum w[(F_{o})^{2}-$	$(F_c)^2$ ] <sup>2</sup> / $\sum w$

**2.3. Physical Properties.** The largest crystals of each batch were selected for physical property measurements. Temperature-dependent DC magnetization data were collected using a Quantum Design MPMS system. Samples were zero-field cooled (ZFC) and then measured on warming from 2–300 K in an external magnetic field of 0.02 T for Pr and Nd analogues and 0.2 T for Sm analogue. The magnetization versus applied field was measured at 5 K in fields between  $\pm 7$  T. The electrical resistance of the polyhedral single crystals was measured using the AC transport option in a Quantum Design PPMS system. A standard 4-probe method was used, where electrical contacts to the sample consisted of 2-mil diameter Pt wire attached with Epotek H20E conductive epoxy.

#### 3. RESULTS

**3.1. Structure.**  $Ln_2Co_3Ge_5$  (Ln = Pr, Nd, and Sm) crystallizes in the monoclinic  $Lu_2Co_3Si_5$ -type structure<sup>13</sup> with the C2/c space group (Figure 2). The  $Lu_2Co_3Si_5$  type structure is a distorted variant of the orthorhombic  $U_2Co_3Si_5$ -type<sup>12</sup> consisting of seven crystallographic sites. The structural relationship between  $U_2Co_3Si_5$  and  $Lu_2Co_3Si_5$  becomes evident when the  $Lu_2Co_3Si_5$ -type structure is described in the nonstandard space group I2/c (Figure SI4).<sup>13</sup> For the  $Lu_2Co_3Si_5$ -type structure in I2/c, the angle  $\beta$ , which is exactly

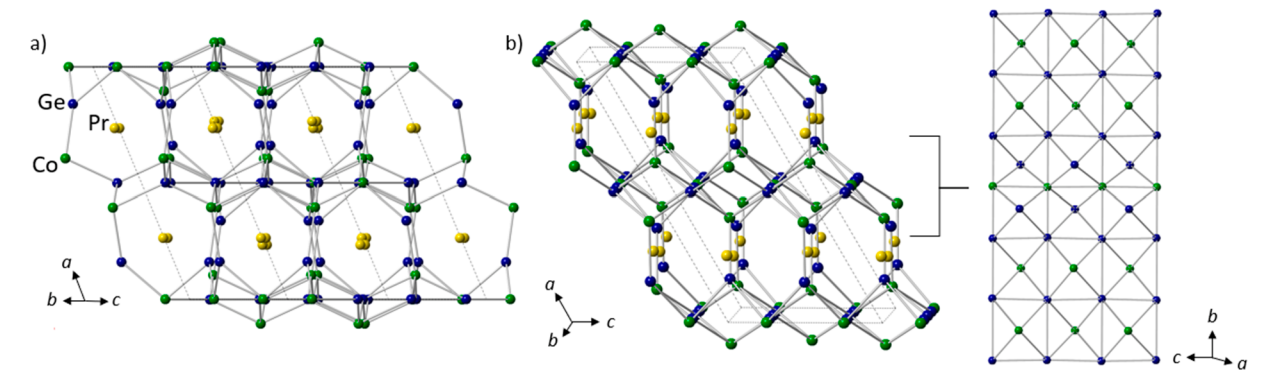


Figure 2. Crystal structure of  $Pr_2Co_3Ge_5(C2/c)$  shown (a) through the face of the Pr polyhedra to show the relationship to the BaAl<sub>4</sub> prototype structure and (b) along the *b* axis with the  $[Co_3Ge_5]$  slab to highlight the distorted square nets.

 $90^{\circ}$  in the orthorhombic structure, deviates slightly from  $90^{\circ}$  and can be written as  $90^{\circ}+\delta$ . In the  $Ln_2Co_3Ge_5$  series,  $\delta$  increases with decreasing Ln-radius, which correlates with the orthorhombic variant for  $Ce_2Co_3Ge_5$  and the monoclinic variant for  $Sm_2Co_3Ge_5$  and beyond.  $^{19}$   $Pr_2Co_3Ge_5$  and  $Nd_2Co_3Ge_5$  have been reported in both the  $Lu_2Co_3Si_5$  and  $U_2Co_3Si_5$  structure types based on powder diffraction.  $^{17,19,27}$  The similarity of powder diffraction patterns between the orthorhombic and monoclinic variant could be the reason for the difference in the previous reports. Structure determination from single crystal X-ray diffraction of our flux grown crystals confirm that the Pr and Nd analogues adopt the monoclinic crystal structure at room temperature.

The arc-melting and annealing procedures developed by Fedyna et al. and Layek et al. 15,17 were followed to synthesize Pr<sub>2</sub>Co<sub>3</sub>Ge<sub>5</sub> in the U<sub>2</sub>Co<sub>3</sub>Si<sub>5</sub> structure type. Still, only the Lu<sub>2</sub>Co<sub>3</sub>Si<sub>5</sub>-type structure was obtained based on powder diffraction data. BaAl<sub>4</sub> derivatives, including the orthorhombic  $Ln_2Pd_3Ge_5$ , have previously been described as  $[M-X]^{\delta-}$  polyanionic networks.<sup>14</sup> In  $Ln_2Co_3Ge_5$ , this network consists of [Co<sub>3</sub>Ge<sub>5</sub>] slabs based on a distorted square net of Co and Ge which are stacked along the a-direction. Alternating capping of the distorted square nets along the b- and cdirection results in interconnections between the [Co<sub>3</sub>Ge<sub>5</sub>] slabs along the a-direction. The lanthanide atoms reside between the [Co<sub>3</sub>Ge<sub>5</sub>] slabs, which gives rise to distorted, irregular icosahedra comprised of Co and Ge atoms around Ln. The distorted square nets in the b-c plane at the center of the [Co<sub>3</sub>Ge<sub>5</sub>] slabs are comprised of Co<sub>2</sub>, Ge<sub>2</sub>, and Ge<sub>4</sub> atoms, with Co1 and Ge1 as the capping atoms. A zigzag chain of the Ge1, Ge2, and Ge4 atoms extends along the c-axis. The Zintl-Klemm concept was applied to a similar compound, La<sub>2</sub>Pd<sub>3</sub>Ge<sub>5</sub>, but it was determined not to be applicable.<sup>28</sup> Further connections of the Lu<sub>2</sub>Co<sub>3</sub>Si<sub>5</sub>- and the U<sub>2</sub>Co<sub>3</sub>Si<sub>5</sub>-type structures to the other variants of the BaAl<sub>4</sub>-type structure become apparent by comparison to the ThCr<sub>2</sub>Si<sub>2</sub>- and the BaNiSn<sub>3</sub>-type structures. These structural relations will be discussed in detail later. Next, we present the physical properties of the Ln<sub>2</sub>Co<sub>3</sub>Ge<sub>5</sub> analogues.

**3.2.** Physical Properties. The temperature-dependent magnetic susceptibility  $\chi = M/H$  of  $Pr_2Co_3Ge_5$  presented in Figure 3a (inset) shows a magnetic transition at 33 K. A spin reorientation occurs at 27 K, as evident by a plateau in the susceptibility, followed by a further increase of the susceptibility,  $\chi$ , before an antiferromagnetic-like cusp at 6 K. A linear fit corresponding to the Curie–Weiss law is applied to the paramagnetic region of the inverse susceptibility  $1/\chi$  between

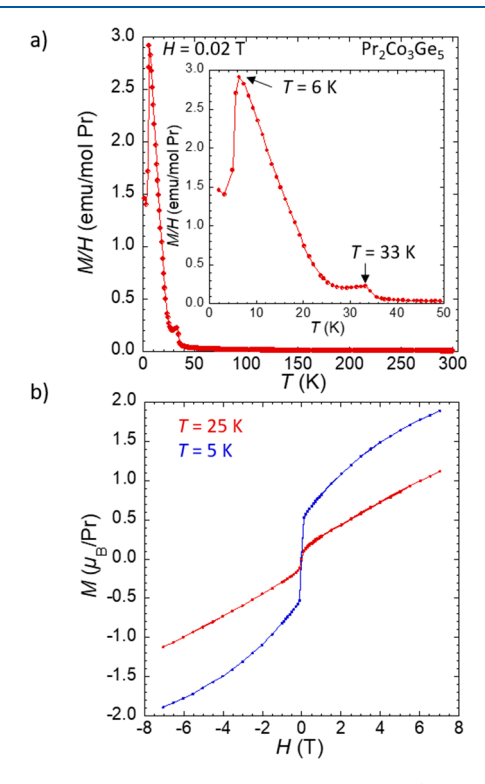
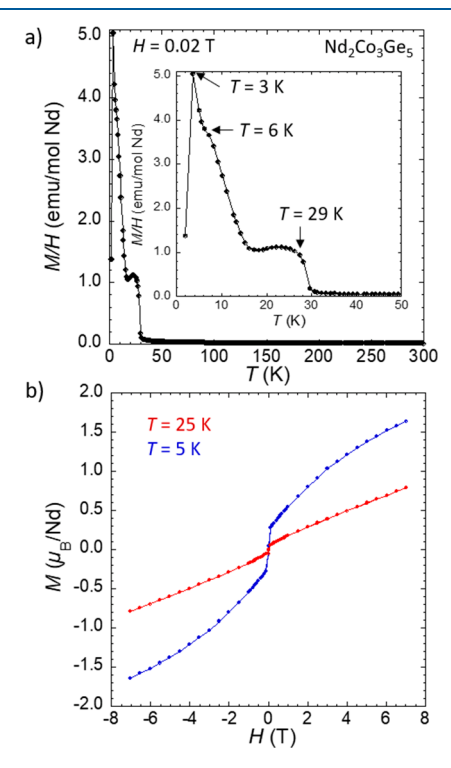


Figure 3. Temperature-dependent magnetization (a) and the field-dependent magnetization (b) of  $\rm Pr_2Co_3Ge_5$ . The inset shows the low temperature range up to 50 K.

60-300 K (Figure SI5). The effective moment obtained from the fit is  $\mu_{\rm eff}$  = 3.52  $\mu_{\rm B}/{\rm Pr}$  atom is in good agreement with the theoretical expected moment for  $Pr^{3+}$  of 3.57  $\mu_B$  suggesting the moment is solely from the lanthanide. This contrasts with prior reports of orthorhombic  $Pr_2Co_3Ge_5$  measured at H = 1 T, which was paramagnetic down to 2 K with  $\mu_{\text{eff}} = 3.76 \ \mu_{\text{B}}/\text{Pr}$ atom and a Weiss constant of  $\Theta$  = 5.48 K. The authors noted a deviation from the Curie-Weiss fit below 50 K, but this was attributed to crystal field effects. 15 At 5 K, the field-dependent magnetization shows a rapid increase upon application of a small external magnetic field H up to 0.025 T (see Figure 3b and Figure SI6). Beyond H = 0.025 T, the magnetization Mincreases more slowly, but does not saturate up to 7 T. Similarly, the field-dependent magnetization at 25 K increases sharply, then increases steadily, reminiscent of the metamagnetic transitions found in PrCo<sub>2</sub>Ge<sub>2</sub>.<sup>29,30</sup>

The temperature-dependent magnetization of Nd<sub>2</sub>Co<sub>3</sub>Ge<sub>5</sub> is shown in the inset of Figure 4a. The susceptibility increases



**Figure 4.** Temperature-dependent magnetization (a) and the field-dependent magnetization (b) of Nd<sub>2</sub>Co<sub>3</sub>Ge<sub>5</sub>. The inset shows the low temperature range up to 50 K.

below 29 K and plateaus between 15 and 25 K. Upon further cooling, a shoulder is observed at 6 K and the magnetization increases followed by a downturn below 3 K. We note that the inverse magnetic susceptibility shows a slight deviation from a linear behavior in the temperature range of 130–165 K (Figure SI5b), though not intrinsic to the sample as no anomaly was observed in the resistivity. The Weiss constant  $\Theta$  is -8.7 K, signaling predominantly antiferromagnetic interactions. Surprisingly, the effective moment  $\mu_{\rm eff}$  is 4  $\mu_{\rm B}/{\rm Nd}$  atom, larger than the expected moment for Nd<sup>3+</sup> of 3.62  $\mu_{\rm B}$  (Figure SI5). The field-dependent magnetization M of Nd<sub>2</sub>Co<sub>3</sub>Ge<sub>5</sub> is similar to the Pr-analogue at both 5 and 25 K, respectively, and does not saturate up to 7 T. As shown in Figure 4b and Figure SI6, a jump in magnetization is also seen for the Nd-analogue at H = 0.025 T, and the magnetization does not reach saturation.

The temperature-dependent susceptibility  $\chi$  of  $\mathrm{Sm_2Co_3Ge_5}$  is presented in Figure 5a. A magnetic transition can be seen at 26 K followed by a small upturn of the susceptibility below 6 K that could be attributed to a spin reorientation. The inverse susceptibility  $1/\chi$  (see Figure SI5 and Figure SI7) follows a modified Curie—Weiss law (1) with a large diamagnetic contribution of  $\chi_0 = -1.4(1) \times 10^{-3}$  emu/mol.

$$\chi = \chi_0 + \frac{C}{T - \Theta} \tag{1}$$

The Weiss constant  $\Theta$  for  $\mathrm{Sm_2Co_3Ge_5}$  is 22.8 K, and the experimentally obtained effective moment is 1.03  $\mu_{\mathrm{B}}/\mathrm{Sm}$  atom, slightly higher than the theoretical moment of 0.85  $\mu_{\mathrm{B}}/\mathrm{Sm}^{3+}$ . As shown in Figure 5b, the magnetization M increases linearly with increasing strength of the external applied field H, consistent with the antiferromagnetic behavior at 5 K.

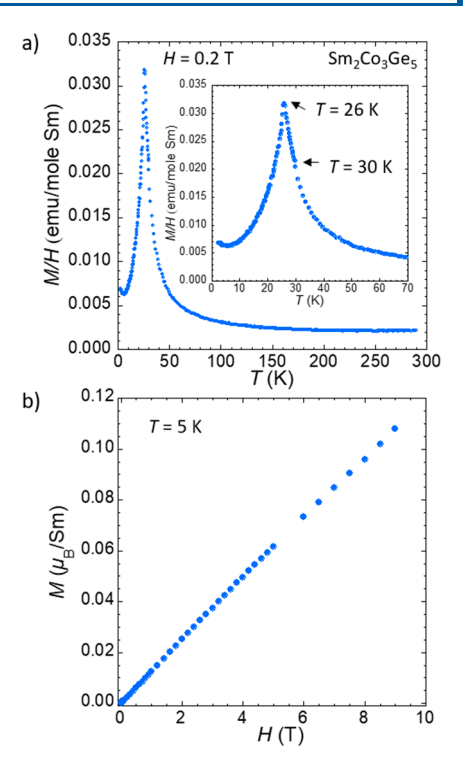


**Figure 5.** Temperature-dependent magnetization (a) and the field-dependent magnetization (b) of  $Sm_2Co_3Ge_5$ . The inset shows the low temperature range from 0 to 70 K.

The normalized temperature dependent resistivities of  $Ln_2Co_3Ge_5$  (Ln = Pr, Nd, and Sm) are presented in Figure 6. The resistivity R(T) has been normalized by  $R_0(T=250 \text{ K})$ .

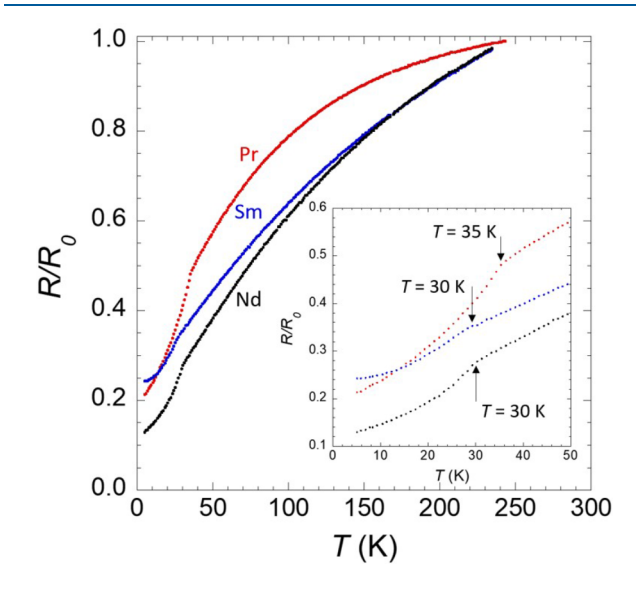


**Figure 6.** Normalized temperature dependent resistivity of Pr<sub>2</sub>Co<sub>3</sub>Ge<sub>5</sub> (red), Nd<sub>2</sub>Co<sub>3</sub>Ge<sub>5</sub> (black), and Sm<sub>2</sub>Co<sub>3</sub>Ge<sub>5</sub> (blue). The temperature range below 50 K is magnified in the inset.

The compounds are metallic but deviate from a linear behavior, potentially indicating Kondo screening. A change of slope occurs in the range of 29–35 K which coincides well with the ordering temperatures observed in the temperature-dependent magnetization data. However, the observed spin reorientations are not reflected in the temperature-dependent resistivity. The residual resistivity ratios (RRR) of these

**Inorganic Chemistry** Article pubs.acs.org/IC

compounds are in the range of 4-10. Next, we compare the properties of the Ln<sub>2</sub>Co<sub>3</sub>Ge<sub>5</sub> analogues to those of LnCoGe<sub>3</sub> and LnCo<sub>2</sub>Ge<sub>2</sub> to establish their structural relationship and correlate their physical properties.

### 4. DISCUSSION

The U<sub>2</sub>Co<sub>3</sub>Si<sub>5</sub><sup>12</sup> and Lu<sub>2</sub>Co<sub>3</sub>Si<sub>5</sub><sup>13</sup> structure types are both compositionally and structurally intermediate to the ThCr<sub>2</sub>Si<sub>2</sub> and BaNiSn<sub>3</sub> structures. While the CaBe<sub>2</sub>Ge<sub>2</sub> structure type is more fitting to describe the U<sub>2</sub>Co<sub>3</sub>Si<sub>5</sub> structure, since it is not stabilized in the Ln-CoGe system, the ThCr<sub>2</sub>Si<sub>2</sub> was selected instead.<sup>34</sup> In the present case, the ThCr<sub>2</sub>Si<sub>2</sub> and BaNiSn<sub>3</sub> structures correspond to LnCo<sub>2</sub>Ge<sub>2</sub> and LnCoGe<sub>3</sub>, respectively. The [Co<sub>3</sub>Ge<sub>5</sub>] capped square net slab of the U<sub>2</sub>Co<sub>3</sub>Si<sub>5</sub> structure can be described as a combination of both the [Co<sub>2</sub>Ge<sub>2</sub>] slab, as found in ThCr<sub>2</sub>Si<sub>2</sub>, and the [CoGe<sub>3</sub>] slab of the BaNiSn<sub>3</sub>. Crystallographically, this manifests as two unique Co sites, seen in Figure SI8, corresponding to the different Co sites in ThCr<sub>2</sub>Si<sub>2</sub> and BaNiSn<sub>3</sub>. The two building blocks repeat in sets of two along the b-direction as seen in Figure 7b,

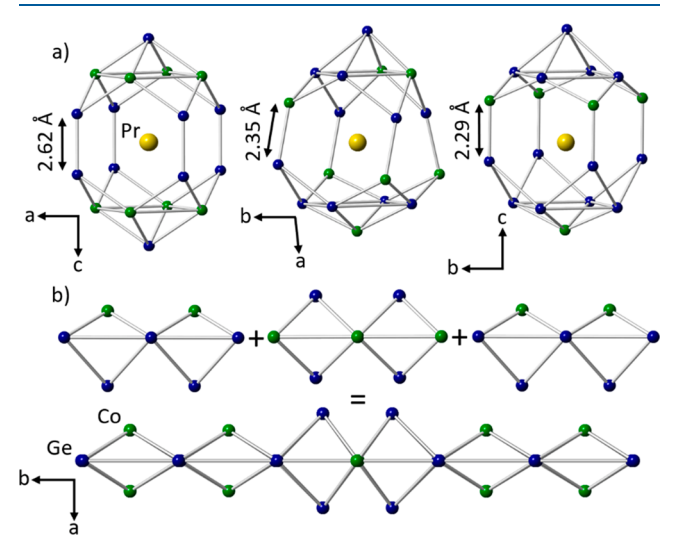


Figure 7. (a) Praseodymium local environment of PrCo<sub>2</sub>Ge<sub>2</sub> (left), Pr<sub>2</sub>Co<sub>3</sub>Ge<sub>5</sub> (middle), and PrCoGe<sub>3</sub> (right). (b) Projection along the c axis of the hybrid distorted square net structure in Pr<sub>2</sub>Co<sub>3</sub>Ge<sub>5</sub> built from a PrCoGe<sub>3</sub>, a PrCo<sub>2</sub>Ge<sub>2</sub>, and an additional PrCoGe<sub>3</sub> square net unit in order of appearance.

resulting in slightly corrugated layers of Ln-atoms parallel to the bc-plane, contrasting with the planar Ln-layers of LnCo<sub>2</sub>Ge<sub>2</sub> and LnCoGe<sub>3</sub> (Figure SI9.). As such, the average intralayer distance between the Ln-atoms increases from 4.0 Å in LnCo<sub>2</sub>Ge<sub>2</sub>, to 4.2 Å in Ln<sub>2</sub>Co<sub>3</sub>Ge<sub>5</sub>, and 4.3 Å in LnCoGe<sub>3</sub> (see Table 2). This is consistent with a stepwise substitution of the smaller Co in the square nets of LnCo<sub>2</sub>Ge<sub>2</sub> with the larger Ge square nets of Ln<sub>2</sub>Co<sub>3</sub>Ge<sub>5</sub> and LnCoGe<sub>3</sub>. In contrast, the average interlayer distance does not increase monotonically, but it is the shortest for Ln<sub>2</sub>Co<sub>3</sub>Ge<sub>5</sub>. The monoclinic distortion is accompanied by a tilt of the Co-Ge dimer formed by the apical atoms of adjacent [Co<sub>3</sub>Ge<sub>5</sub>] slabs as emphasized in Figure 7a. A similar dimer is observed in LnCoGe3; however, the corresponding bond distance in Ln<sub>2</sub>Co<sub>3</sub>Ge<sub>5</sub> is significantly longer than the bond distance in LnCoGe3. Additionally, LnCoGe<sub>3</sub> in the BaNiSn<sub>3</sub>-type structure has been observed experimentally only for the early rare-earth elements (Ln = La- Eu), whereas the  $Ln_2Co_3Ge_5$  is observed for Ln = La - Er.

Ln compound	T, (K)	T, (K)	T, (K)	T, (K) T, (K) T <sub>2</sub> (K) avg. $\Theta$ (K) fit range (K)	fit range (K)	exp. $\mu_{eff}$ ( $\mu_{\rm B}/{\rm Ln}$ )	exp. $\mu_{eff}(\mu_B/Ln)$ theo. $\mu_{eff}(\mu_B/Ln)$	H, (T)	H, (T) H, (T)		avg. interlayer (Å) avg. intralayer (Å)	avg. diagonal (Å)	
Pr									,				
$PrCo_2Ge_2$	27	<1.8		-23		3.5	3.57	0.5°	$2^c$	5.866	4.056	5.736	
$Pr_2Co_3Ge_5$	33	9		6.0	60-300	3.52		0.02		5.730	4.186	5.912	
$PrCoGe_3$				-5.7	150-300	3.55 <sup>a</sup>		$50^c$		5.782	4.308	6.093	
PN													
$NdCo_2Ge_2$	28	6		-19		3.6	3.62	$1.7^{c}$		5.826	4.037	5.709	
$Nd_2Co_3Ge_5$	53	9	ъ	-8.7	175-300	4		0.03		5.714	4.176	5.897	
$NdCoGe_3$			3.8	-12	200-300	3.62		$1.7^{b}$		5.772	4.296	9.076	
Sm													
SmCo <sub>2</sub> Ge <sub>2</sub>	17						0.85			5.788	4.006	5.665	
$\mathrm{Sm}_{2}\mathrm{Co}_{3}\mathrm{Ge}_{5}$	79			22.8	50 200	1.03				5.717	4.155	5.834	
$SmCoGe_3$													

This work. "Average." Measured along the crystallographic a axis. "Measured along the crystallographic c axis." Where  $T_i$  (i=1,2,3) are the ordering temperatures, fit range is the temperature range of (i = 1, 2) are obtained from the field dependent magnetization. All constants obtained for LnCo<sub>2</sub>Ge, and LnCoGe<sub>3</sub> were given from the cited references. The average interlayer, intralayer, and diagonal distances are obtained from the crystal the Curie-Weiss fit,  $\Theta$  is the Weiss constant, and  $\mu_{eff}$  is experimental and theoretical effective magnetic moment for each Ln-analogue. Metamagnetic transitions  $H_1$ 

structures of Ln<sub>2</sub>Co<sub>3</sub>Ge<sub>5</sub>, LnCo<sub>2</sub>Ge<sub>2</sub>, and LnCoGe<sub>3</sub>

The decreasing radius of the rare-earth atoms forces a decreasing dimer bond distance, resulting in very short Co–Ge bonds in the apical dimer of the BaNiSn<sub>3</sub>-type structure, which limits their stability under ambient pressure to the larger rare-earth elements. The tilting of the Co–Ge dimer in the monoclinic Lu<sub>2</sub>Co<sub>3</sub>Si<sub>5</sub>-type structure alleviates the chemical pressure and allows the formation of Ln<sub>2</sub>Co<sub>3</sub>Ge<sub>5</sub> compounds with rare-earth elements smaller than Eu. The three crystal structures are very intertwined and are distinct by small structural differences. Next, we analyze the effects of these small differences on their physical properties.

The magnetic susceptibility of Sm<sub>2</sub>Co<sub>3</sub>Ge<sub>5</sub> above the magnetic ordering temperature is remarkably similar to SmCo<sub>2</sub>Ge<sub>2</sub> and does not obey Curie-Weiss Law, possibly due to thermal population of Hund's rule excited states.<sup>29</sup> The effective magnetic moment of Sm<sub>2</sub>Co<sub>3</sub>Ge<sub>5</sub> obtained from the modified Curie-Weiss fit is greater than the expected Sm<sup>3+</sup> moment, possibly due to Co contribution. Similarities in the magnetic and transport properties between Ln<sub>2</sub>Co<sub>3</sub>Ge<sub>5</sub>, LnCoGe3, and LnCo2Ge2 are present for the Pr and Nd analogues as well, most notably in the ordering temperatures and in the field strength H where metamagnetic transitions occur as seen in Table 2. There is another metamagnetic transition at 10 T previously reported from experimental data for PrCo<sub>2</sub>Ge<sub>2</sub>, which is not listed in Table 2.30 The magnetic moments of the Pr analogues all agree with a Pr3+ state; however, Nd<sub>2</sub>Co<sub>3</sub>Ge<sub>5</sub> shows an elevated magnetic moment compared to what is expected for Nd3+, which is unlike NdCoGe<sub>3</sub> and NdCo<sub>2</sub>Ge<sub>2</sub>. Another key difference between the properties of these compounds is seen in the resistivity. In Ln<sub>2</sub>Co<sub>3</sub>Ge<sub>5</sub>, the temperature-dependent resistivity does not increase linearly, as in both LnCoGe<sub>3</sub> and LnCo<sub>2</sub>Ge<sub>2</sub>. This curvature could be indicative of Kondo scattering, or it could be due to crystal field effects in Pr<sub>2</sub>Co<sub>3</sub>Ge<sub>5</sub> as previously suggested. 15 Since Ln<sub>2</sub>Co<sub>3</sub>Ge<sub>5</sub> is structurally and compositionally intermediate to LnCoGe<sub>3</sub> and LnCo<sub>2</sub>Ge<sub>2</sub>, these structures can be used as a system to study the suppression of Kondo scattering in lanthanide cobalt germanides. Finally, the differences in magnetic behavior we see across the structure types could be a result of subtle changes in the local environment of the Ln atom impacting their crystal field splitting. Although the field dependent magnetization of Ln<sub>2</sub>Co<sub>3</sub>Ge<sub>5</sub> (Ln = Pr, Nd) are reminiscent of the reported PrCoGe<sub>3</sub> and NdCoGe<sub>3</sub>, the transition temperatures of the Ln<sub>2</sub>Co<sub>3</sub>Ge<sub>5</sub> are higher and metamagnetic transitions occur at lower fields. CEF effects can be attributed to the ground state behavior for both structure types, and the distortion about the lanthanides is significant to the magnetic phase transitions.<sup>33</sup>

# 5. CONCLUSION

In this paper, we presented the magnetic susceptibility, resistivity, flux growth synthesis, and crystal structures of  $Pr_2Co_3Ge_5$ ,  $Nd_2Co_3Ge_5$ , and  $Sm_2Co_3Ge_5$ , which crystallize in the monoclinic  $Lu_3Co_3Si_5$ -type structure. The structure is a derivative of the  $BaAl_4$ -type structure and, as such, contains distorted square nets. The square net motif presents itself in many topological materials, such as  $TaAs^{35}$  and  $LaAlGe_5^{36}$  and has been correlated with the presence of topological band structures. The potential for rare earth germanide ternary compounds to host magnetic topological states, as seen in  $LnAlGe_5$  ( $Ln = Ce_5$ ,  $Pr_5$ ), is exciting and merits further investigation of the  $BaAl_4$ -related phases.

#### ASSOCIATED CONTENT

# Supporting Information

The Supporting Information is available free of charge at https://pubs.acs.org/doi/10.1021/acs.inorgchem.1c01978.

(PDF)

### **Accession Codes**

CCDC 2088447–2088449 contain the supplementary crystallographic data for this paper. These data can be obtained free of charge via <a href="www.ccdc.cam.ac.uk/data\_request/cif">www.ccdc.cam.ac.uk/data\_request/cif</a>, or by emailing <a href="mailto:data\_request@ccdc.cam.ac.uk">data\_request@ccdc.cam.ac.uk</a>, or by contacting The Cambridge Crystallographic Data Centre, 12 Union Road, Cambridge CB2 1EZ, UK; fax: +44 1223 336033.

### AUTHOR INFORMATION

# **Corresponding Author**

Julia Y. Chan — Department of Chemistry and Biochemistry, University of Texas at Dallas, Richardson, Texas 75080, United States; orcid.org/0000-0003-4434-2160; Email: Julia.Chan@utdallas.edu

#### **Authors**

Trent M. Kyrk – Department of Chemistry and Biochemistry, University of Texas at Dallas, Richardson, Texas 75080, United States

Jan P. Scheifers – Department of Chemistry and Biochemistry, University of Texas at Dallas, Richardson, Texas 75080, United States

Kulatheepan Thanabalasingam — Department of Chemistry and Biochemistry, University of Texas at Dallas, Richardson, Texas 75080, United States; orcid.org/0000-0002-5110-7030

Gregory T. McCandless – Department of Chemistry and Biochemistry, University of Texas at Dallas, Richardson, Texas 75080, United States

David P. Young – Department of Physics and Astronomy, Louisiana State University, Baton Rouge, Louisiana 70803-4001, United States

Complete contact information is available at: https://pubs.acs.org/10.1021/acs.inorgchem.1c01978

#### **Author Contributions**

T. M. K., J. P. S., and K.T. are joint first-authors of the manuscript and contributed equally. They are listed in the order of the lanthanide they handled for the work presented (T. M. K., Pr; J. P. S., Nd; and K.T., Sm).

#### Notes

The authors declare no competing financial interest.

## ACKNOWLEDGMENTS

This work was partially supported by the National Science Foundation (DMR-1700030) and the Welch Foundation (AT-2056-20210327). D. P. Y. acknowledges support from the NSF under Grant No. DMR-1904636. The authors acknowledge Ms. Leah Thompson, the Department of Geosciences, University of Texas at Dallas, for assisting with the EDS elemental analysis of all three samples.

#### REFERENCES

(1) Wang, K.; Mori, R.; Wang, Z.; Wang, L.; Ma, J. H. S.; Latzke, D. W.; Graf, D. E.; Denlinger, J. D.; Campbell, D.; Bernevig, B. A.; Lanzara, A.; Paglione, J. Crystalline Symmetry-Protected Non-Trivial

- Topology in Prototype Compound BaAl<sub>4</sub>. npj Quantum Mater. 2021, 6, No. 28.
- (2) Xu, Y.; Elcoro, L.; Song, Z.-D.; Wieder, B. J.; Vergniory, M. G.; Regnault, N.; Chen, Y.; Felser, C.; Bernevig, B. A. High-Throughput Calculations of Magnetic Topological Materials. *Nature* **2020**, 586, 702–707.
- (3) Settai, R.; Okuda, Y.; Sugitani, I.; Onuki, Y.; Matsuda, T. D.; Haga, Y.; Harima, H. Non-Centrosymmetric Heavy Fermion Superconductivity in CeCoGe<sub>3</sub>. *Int. J. Mod. Phys. B* **2007**, *21*, 3238–3245.
- (4) Ivanov, V.; Wan, X.; Savrasov, S. Y. Renormalized Quasiparticles, Topological Monopoles, and Superconducting Line Nodes in Heavy-Fermion CeTX<sub>3</sub> Compounds. *Phys. Rev. B: Condens. Matter Mater. Phys.* **2021**, *103*, L041112.
- (5) Weiland, A.; Felder, J. B.; McCandless, G. T.; Chan, J. Y. One Ce, Two Ce, Three Ce, Four? An Intermetallic Homologous Series to Explore:  $A_{n+1}B_nX_{3n+1}$ . *Chem. Mater.* **2020**, *32*, 1575–1580.
- (6) Sung, N. H.; Roh, C. J.; Kim, K. S.; Cho, B. K. Possible Multigap Superconductivity and Magnetism In Single Crystals of Superconducting La<sub>2</sub>Pt<sub>3</sub>Ge<sub>5</sub> and Pr<sub>2</sub>Pt<sub>3</sub>Ge<sub>5</sub>. *Phys. Rev. B: Condens. Matter Mater. Phys.* **2012**, *86*, 224507.
- (7) Sheng, Q; Zhang, J; Huang, K; Ding, Z; Peng, X; Tan, C; Shu, L Superconductivity in Self-Flux-Synthesized Single Crystalline  $R_2Pt_3Ge_5$  (R = La, Ce, Pr). Chin. Phys. B **2017**, 26, 057401.
- (8) Kaushik, V.; Venkateshwarlu, D.; Mishra, A. K.; Krishnan, M.; Venkatesh, R.; Patidar, M. M.; Ganesan, V. Robust Superconductivity Against The Antiferromagnetic Ordering in Pr<sub>2</sub>Pt<sub>3</sub>Ge<sub>5</sub>. *Phys. B* **2019**, 570, 296–300.
- (9) Bugaris, D. E.; Malliakas, C. D.; Han, F.; Calta, N. P.; Sturza, M.; Krogstad, M. J.; Osborn, R.; Rosenkranz, S.; Ruff, J. P. C.; Trimarchi, G.; Bud'ko, S. L.; Balasubramanian, M.; Chung, D. Y.; Kanatzidis, M. G. Charge Density Wave in the New Polymorphs of RE<sub>2</sub>Ru<sub>3</sub>Ge<sub>5</sub> (RE = Pr, Sm, Dy). *J. Am. Chem. Soc.* **2017**, *139*, 4130–4143.
- (10) Kuo, C. N.; Hsu, C. J.; Tseng, C. W.; Chen, W. T.; Lin, S. Y.; Liu, W. Z.; Kuo, Y. K.; Lue, C. S. Charge Density Wave Like Behavior With Magnetic Ordering in Orthorhombic Sm<sub>2</sub>Ru<sub>3</sub>Ge<sub>5</sub>. *Phys. Rev. B: Condens. Matter Mater. Phys.* **2020**, *101*, 155140.
- (11) Bugaris, D. E.; Malliakas, C. D.; Bud'ko, S. L.; Calta, N. P.; Chung, D. Y.; Kanatzidis, M. G. Flux Crystal Growth of the  $RE_2Ru_3Ge_5$  (RE = La, Ce, Nd, Gd, Tb) Series and Their Magnetic and Metamagnetic Transitions. *Inorg. Chem.* **2017**, *56*, 14584–14595.
- (12) Aksel'rud, L. G.; Yarmolyuk, Y. P.; Gladyshevskij, E. I. Kristallicheskaya structure soedineniya U<sub>2</sub>Co<sub>3</sub>Si<sub>5</sub>. *Kristallografiya* 1977, 22, 861.
- (13) Chabot, B.; Parthé, E. Dy<sub>2</sub>Co<sub>3</sub>Si<sub>5</sub>, Lu<sub>2</sub>Co<sub>3</sub>Si<sub>5</sub>, Y<sub>2</sub>Co<sub>3</sub>Si<sub>5</sub> and Sc<sub>2</sub>Co<sub>3</sub>Si<sub>5</sub> with a Monoclinic Structural Deformation Variant of The Orthorhombic U<sub>2</sub>Co<sub>3</sub>Si<sub>5</sub> Structure Type. *J. Less-Common Met.* **1985**, 106, 53–59.
- (14) Solokha, P.; Freccero, R.; De Negri, S.; Proserpio, D. M.; Saccone, A. The  $R_2Pd_3Ge_5$  (R = La-Nd, Sm) Germanides: Synthesis, Crystal Structure and Symmetry Reduction. *Struct. Chem.* **2016**, *27*, 1693–1701.
- (15) Layek, S.; Anand, V. K.; Hossain, Z. Valence Fluctuation in  $Ce_2Co_3Ge_5$  and Crystal Field Effect in  $Pr_2Co_3Ge_5$ . *J. Magn. Magn. Mater.* **2009**, 321, 3447–3452.
- (16) Soudé, A.; Pikul, A. P.; Wiśniewski, P.; Tougait, O.; Pasturel, M.; Kaczorowski, D.; Noël, H. Magnetic, Electric and Thermoelectric Properties of Ternary Intermetallics From The Ce-Co-Ge System. *Intermetallics* **2011**, *19*, 1201–1206.
- (17) Fedyna, M.; Pecharskii, V.; Bodak, O. New Ternary Praseodymium Germanides. *Inorg. Mater.* (USSR) **1987**, 23, 570–574.
- (18) Salamakha, P. Interaction of Neodymium and Germanium with d-Elements. Phase Diagrams and Crystal Structure of Ternary Compounds. *J. Alloys Compd.* **1997**, 255, 209–220.
- (19) Venturini, G.; Méot-Meyer, M.; Marêché, J. F.; Malaman, B.; Roques, B. De Nouveaux Isotypes de U<sub>2</sub>Co<sub>3</sub>Si<sub>5</sub> ou Lu<sub>2</sub>Co<sub>3</sub>Si<sub>5</sub> Dans les Systems R-T-Ge (R = Elements Des Terres Rares; T = Ru, Co, Rh, Ir). Supraconductivite de Y<sub>2</sub>Ir<sub>3</sub>Ge<sub>5</sub>. *Mater. Res. Bull.* **1986**, 21, 33–39.

- (20) Pearson's Crystal Data: Crystal Structure Database for Inorganic Compounds. ASM International: Materials Park, OH, USA, 2010.
- (21) Canfield, P.; Kong, T.; Kaluarachchi, U.; Jo, N. H. Use of Fritdisc Crucibles for Routine and Exploratory Solution Growth of Single Crystalline Samples. *Philos. Mag.* **2016**, *96*, 84–92.
- (22) Krause, L.; Herbst-Irmer, R.; Sheldrick, G. M.; Stalke, D. Comparison of Silver and Molybdenum Microfocus X-Ray Sources for Single-Crystal Structure Determination. *J. Appl. Crystallogr.* **2015**, 48, 3–10.
- (23) Sheldrick, G. SHELXT Integrated Space-Group and Crystal-Structure Determination. *Acta Crystallogr., Sect. A: Found. Adv.* **2015**, 71, 3–8.
- (24) Sheldrick, G. Crystal Structure Refinement With SHELXL. Acta Crystallogr., Sect. C: Struct. Chem. 2015, 71, 3–8.
- (25) Sheldrick, G. CELL\_NOW, Version 2008/4; Georg-August-Universität Göttingen: Göttingen, Germany. 2008.
- (26) Sheldrick, G. TWINABS, Version 2012/1; Georg-August-Universität Göttingen: Göttingen, Germany, 2012.
- (27) Salamakha, P. S.; Sologub, O. L.; Bodak, O. I., Chapter 173 Ternary Rare-Earth-Germanium Systems. In *Handbook on the Physics and Chemistry of Rare Earths*; Elsevier: 1999; Vol. 27, pp 1–223.
- (28) Freccero, R.; De Negri, S.; Rogl, G.; Binder, G.; Michor, H.; Rogl, P. F.; Saccone, A.; Solokha, P. La<sub>2</sub>Pd<sub>3</sub>Ge<sub>5</sub> and Nd<sub>2</sub>Pd<sub>3</sub>Ge<sub>5</sub> Compounds: Chemical Bonding and Physical Properties. *Inorg. Chem.* **2021**, *60*, 3345–3354.
- (29) Kong, T.; Cunningham, C. E.; Taufour, V.; Budko, S. L.; Buffon, M. L. C.; Lin, X.; Emmons, H.; Canfield, P. C. Thermodynamic and Transport Properties of Single Crystalline  $RCo_2Ge_2$  (R = Y, La-Nd, Sm-Tm). *J. Magn. Magn. Mater.* **2014**, 358–359, 212–227.
- (30) Vejpravová, J.; Prokleška, J.; Sechovský, V. High-Field Metamagnetism of Giant Anisotropy Antiferromagnet PrCo<sub>2</sub>Ge<sub>2</sub>. *J. Phys.: Conf. Ser.* **2006**, *S1*, 143–146.
- (31) Szytula, A.; Leciejewicz, J.; Bińczycka, H. Crystal and Magnetic Structures of PrCo<sub>2</sub>Ge<sub>2</sub> and HoCo<sub>2</sub>Ge<sub>2</sub>. *Phys. Status Solidi A* **1980**, *58*, 67–70.
- (32) Kawai, T.; Muranaka, H.; Endo, T.; Duc Dung, N.; Doi, Y.; Ikeda, S.; Matsuda, T. D.; Haga, Y.; Harima, H.; Settai, R.; Onuki, Y. Split Fermi Surface Properties of LaTGe<sub>3</sub> (T: Transition Metal) and PrCoGe<sub>3</sub> with the Non-Centrosymmetric Crystal Structure. *J. Phys. Soc. Jpn.* **2008**, *77*, 064717.
- (33) Méasson, M.-a.; Muranaka, H.; Kawai, T.; Ota, Y.; Sugiyama, K.; Hagiwara, M.; Kindo, K.; Takeuchi, T.; Shimizu, K.; Honda, F.; Settai, R.; Onuki, Y. Magnetic Properties of RCoGe<sub>3</sub> (R: Ce, Pr, and Nd) and Strong Anisotropy of the Upper Critical Field in Noncentrosymmetric Compound CeCoGe<sub>3</sub>. *J. Phys. Soc. Jpn.* **2009**, 78, 124712
- (34) Eisenmann, B. New Structural Variant of The BaAl<sub>4</sub>-Type: The CaBe<sub>2</sub>Ge<sub>2</sub>-Type. Z. Naturforsch., B: J. Chem. Sci. **1972**, 27, 1155–1157.
- (35) Xu, S.-Y.; Belopolski, I.; Alidoust, N.; Neupane, M.; Bian, G.; Zhang, C.; Sankar, R.; Chang, G.; Yuan, Z.; Lee, C.-C.; Huang, S.-M.; Zheng, H.; Ma, J.; Sanchez, D. S.; Wang, B.; Bansil, A.; Chou, F.; Shibayev, P. P.; Lin, H.; Jia, S.; Hasan, M. Z. Discovery of a Weyl Fermion Semimetal and Topological Fermi Arcs. *Science* **2015**, *349*, 613.
- (36) Xu, S.-Y.; Alidoust, N.; Chang, G.; Lu, H.; Singh, B.; Belopolski, I.; Sanchez, D. S.; Zhang, X.; Bian, G.; Zheng, H.; Husanu, M.-A.; Bian, Y.; Huang, S.-M.; Hsu, C.-H.; Chang, T.-R.; Jeng, H.-T.; Bansil, A.; Neupert, T.; Strocov, V. N.; Lin, H.; Jia, S.; Hasan, M. Z. Discovery of Lorentz-Violating Type II Weyl Fermions in LaAlGe. *Sci. Adv.* 2017, 3, No. e1603266.
- (37) Schoop, L. M.; Pielnhofer, F.; Lotsch, B. V. Chemical Principles of Topological Semimetals. *Chem. Mater.* **2018**, *30*, 3155–3176.
- (38) Klemenz, S.; Hay, A. K.; Teicher, S. M. L.; Topp, A.; Cano, J.; Schoop, L. M. The Role of Delocalized Chemical Bonding in Square-Net-Based Topological Semimetals. *J. Am. Chem. Soc.* **2020**, *142*, 6350–6359.

(39) Chang, G.; Singh, B.; Xu, S.-Y.; Bian, G.; Huang, S.-M.; Hsu, C.-H.; Belopolski, I.; Alidoust, N.; Sanchez, D. S.; Zheng, H.; Lu, H.; Zhang, X.; Bian, Y.; Chang, T.-R.; Jeng, H.-T.; Bansil, A.; Hsu, H.; Jia, S.; Neupert, T.; Lin, H.; Hasan, M. Z. Magnetic and Noncentrosymmetric Weyl Fermion Semimetals in the RAIGe family of compounds (R = Rare Earth). *Phys. Rev. B: Condens. Matter Mater. Phys.* 2018, 97, 041104.